A Compact McKibben Muscle Based Bending Actuator for Close-to-Body Application in Assistive Wearable Robots

Martin Tschiersky, Edsko E. G. Hekman, *Member, IEEE*, Dannis M. Brouwer, Just L. Herder, *Member, IEEE*, and Koichi Suzumori, *Member, IEEE*

***Abstract*—In this letter we demonstrate a pneumatic bending actuator for upper-limb assistive wearable robots which uses thin McKibben muscles in combination with a flexure strip. The actuator features both active soft actuation and passive gravity support, and in terms of force transmission bridges the gap between the classic rigid type actuators and the emerging soft actuator technologies. Its flexure strip leverages the high-force low-displacement properties of McKibben muscles towards a large rotational range of motion and reduces localized forces at the attachments. We explain the synthesis method by which these actuators can be obtained and optimized for high specific moment output. Physical specimens of three optimized actuator designs are built and tested on a dedicated experimental setup, verifying the computational models. Furthermore, a proof-of-concept upper-limb assistive wearable robot is presented to illustrate a practical application of this actuator and its potential for close-to-body alignment. We found that based on our currently available components actuators can be built which, given a width of 80 mm, are able to produce a moment exceeding 4 Nm at an arm elevation of 90 deg.**

***Index Terms*—Hydraulic/pneumatic actuators, physically assistive devices, prosthetics and exoskeletons, upper-limb, wearable robots.**

I. Introduction

ASSISTIVE wearable robots are devices that are designed to facilitate functional movements of its wearer. These devices target people suffering from deficient motor function [1]. By providing supporting forces and moments they mitigate the effects of muscular weakness, and thereby restore the ability to perform activities of daily living (ADLs). Thus, they can reduce the need for external help and may enhance social participation [2], [3]. Yet, to this day, active assistive wearable devices exhibit significant shortcomings which prevent their widespread adoption [3]–[7]. Many of these can be traced back to the method of actuation [3] which often determines the overall mechanical structure of the device.

Traditionally, industrial grade actuation components in combination with rigid braces or exoskeletons are used [2]. However, promising new technologies emerge from the field of soft robotics, which increasingly permeate into the field of assistive wearable devices. In comparison to their rigid counterparts soft orthotic systems are generally cheaper, lighter and have lower inertia. Furthermore, due to the absence of a rigid external structure they can feature a lower profile which makes them smaller, and therefore, more portable, easier to conceal and potentially even wearable underneath clothing [1]. These benefits of soft robotic architectures are key advantages to raise the functional and social acceptability [7] of assistive wearable robots in order to promote their widespread adoption for everyday use [1], [2].

The two predominant actuation methods currently used in wearable soft robotic devices are electric and pneumatic actuation [1], [8]. Electric actuation is almost exclusively implemented using cable-based transmission systems, which have the ability to provide high forces and large displacements [1], [3]. Pneumatic actuation, on the other hand, boasts a wide range of diverse implementations and embodiments. The advantages of pneumatic actuators are their low impedance, low weight and high power-to-weight ratio, when the pneumatic source is neglected. However, their main disadvantages are, generally, a low force and/or displacement capability [1].

The exception to this rule are the class of pneumatic artificial muscles (PAMs) which, although limited in stroke, possess high force capabilities. Several different embodiments of PAMs exist, but the most established and most commonly used in wearable robotic devices is the McKibben muscle type actuator [1], [9]. The basic structure of a McKibben muscle comprises a gas-tight elastic inflatable tube or bladder surrounded by a helical braided sleeve composed of flexible, inextensible threads. When pressure is applied, the inner tube expands radially against the braid. Due to the high longitudinal stiffness of the threads the actuator has to shorten for its volume to increase. This causes the actuator to contract and produce tension [9], [10]. Increasing efforts have been made to miniaturize McKibben muscles [11]–[13]. These miniaturized versions feature a reduced size and weight, while

Manuscript received September 10, 2019; accepted January 25, 2020. Date of publication February 21, 2020; date of current version March 2, 2020. This letter was recommended for publication by Associate Editor Michael C. Yip and Editor Paolo Rocco upon evaluation of the reviewers' comments. This work was supported in part by the Japan Society for the Promotion of Science (JSPS) under the FY 2019 JSPS Postdoctoral Fellowship for Research in Japan (Short-term) PE19704, and in part by the European Union's Horizon 2020 Research and Innovation Programme under grant agreement No. 688857 (SoftPro). *(Corresponding author: Martin Tschiersky.)*

Martin Tschiersky and Dannis M. Brouwer are with the Chair of Precision Engineering, University of Twente, 7500 AE Enschede, The Netherlands (e-mail: m.tschiersky@utwente.nl; d.m.brouwer@utwente.nl).

Edsko E. G. Hekman is with the Department of Biomechanical Engineering, University of Twente, 7500 AE Enschede, The Netherlands (e-mail: e.e.g.hekman@utwente.nl).

Just L. Herder is with the Department of Precision and Microsystems Engineering, Delft University of Technology, 2628 CD Delft, The Netherlands (e-mail: j.l.herder@tudelft.nl).

Koichi Suzumori is with the Department of Mechanical Engineering, Tokyo Institute of Technology, Tokyo 152-8552, Japan (e-mail: suzumori@mes.titech.ac.jp).

This letter has supplementary downloadable material available at http://ieeexplore.ieee.org, provided by the authors.

Digital Object Identifier 10.1109/LRA.2020.2975732

maintaining the high specific force and power characteristics. In addition, they stay flexible when pressurized, allowing them to bend while contracting [14]. These features make them exceptionally suitable for use in wearable soft robotic devices, as they enable alignment very close to the body, distribution of actuation across the body surface and organization into larger structures, such as bundles [14], braids [15], weaves [16] and active textiles [17], [18]. Their application to upper-limb soft exosuits was previously shown by Abe *et al.* [16], [19].

However, McKibben muscles – similar to cable-based systems – apply tension forces very localized at their attachment points. This can be a major design challenge for powerful wearable soft robots due to the lack of a rigid frame to bear, redirect and distribute these forces to the wearer's body [1], [20]. Furthermore, to produce functional strokes McKibben muscles require large lengths, resulting in extensive routing across the body which can lead them to slide, apply uncomfortable forces and restrict motion [21].

Therefore, we propose a pneumatic bending actuator (PBA) which uses miniaturized McKibben muscles in combination with a flexure strip to transform the linear displacements and forces into rotational displacements and moments, respectively. Many PBAs dedicated for use in wearable soft robotic devices have been shown in previous works, some of them based on McKibben muscles [22]. However, dedicated research towards PBAs with maximized force or moment output, bending displacement and power density is scarce [23].

We intend to leverage the high-force low-displacement properties of McKibben muscles through a flexure mechanism which is optimized to maximize the moment for lifting the upper arm while enabling a natural range of motion (ROM) and close-to-body alignment. Thereby, we create an actuator which incorporates both active soft actuation and passive gravity assistance, within a structure which exhibits the compliant characteristics of soft robotic devices while featuring an external force transmission behavior comparable to rigid exoskeletons.

Following this introduction we present the actuator design, the computational models, the applied optimization as well as the experiment in the *Methods* section. In the *Results* section the outcomes of both the simulation based optimization and the physical experiment are presented. Furthermore, the application of the actuator to an upper-limb assistive wearable robot is illustrated. The results are further elaborated upon within the *Discussion* section. Lastly, in the *Conclusion* section we concisely summarize all key findings.

II. Methods

A. Application Requirements

The actuator presented in this letter is designated for use in an upper-limb assistive wearable robot to provide active assistance for lifting the arms from a relaxed position at 0 deg elevation to ≥ 90 deg elevation, while passively allowing for a full natural ROM of up to 180 deg elevation. Its primary purpose is to compensate for the weight of the arms. By augmenting the wearers residual force to an elevation, i.e., flexion or abduction, of at least 90 deg it could potentially assist in the execution of the majority of ADLs found in literature [24]. Using the mean body segment data of female and male subjects as provided by [25] we calculate an external gravity moment acting on the shoulder joint of 9.16 Nm when lifting a fully extended arm to 90 deg elevation. During common ADLs maximum shoulder joint moments of up to 14.3 ± 1.4 Nm are encountered [26]. In addition, the actuator is supposed to stay very close to the body and have a low profile. Studies on passive assistive orthoses have shown that devices should generally stay within 30 mm from the body [2], and below 20 mm to be wearable underneath clothing [27]. The actuator is to be fixed to the top of the shoulder and to the upper arm at each end, respectively. These regions are favorable regarding natural self-perception and low obstructiveness [28]. As the actuator should wrap around the shoulder we determined, based on anthropometric data [29] and own estimates, that the minimum bending radius of the actuator should reach 80 mm or less in order to achieve a close fit.

B. Actuator Design

The proposed actuator consists of a straight flexure strip, which is subdivided into serial segments by means of equally spaced brackets that extend unilaterally from the strip. One or multiple miniaturized McKibben muscles run in parallel to the flexure, and are routed through and fixed to the brackets along their height. To avoid buckling, a central portion of the flexure strip can be reinforced by locally increasing the thickness. Multiple actuator strips can be arranged in parallel, either loosely or by physically merging them into one strip.

To enable bi-directional bending, and thus a natural ROM, the fully extended, i.e., the uninflated and unstressed length of the McKibben muscles has to be longer than the flexure length. Therefore, the McKibben muscles are compressed between each pair of brackets, externally applying an initial contraction to the braided sleeve before they are fixed.

When the McKibben muscles are inflated their internal bladder causes them to contract further, and depending on the applied pneumatic pressure and the deflection state of the actuator, exert tension forces onto the brackets. The brackets, effectively acting as levers, transfer these forces to the flexure and induce moments. The actuator reaches an equilibrium state when the moments created by the McKibben muscles, the bending moments of the flexure strip, and the external moment loads are in balance.

C. Materials

For the flexure strip SK85 hardened steel sheets are used. Based on their specified hardness (HRC $42 \sim 46$) a tensile strength of $\sigma_t = 1435$ MPa is determined [30]. The brackets and flexure reinforcement are made from an acrylonitrile-butadiene-styrene (ABS) copolymer [31]. The miniaturized McKibben muscles used in this study are production prototypes provided by s-muscle Co. Ltd. which have an uninflated and inflated diameter 3 and 5 mm, respectively. Their pressure dependent stiffness properties are determined in isobaric quasistatic experiments on a tensile test setup consisting of a COMS PM80B-50X linear precision stage, Nidec-Shimpo FGP-50 digital force gauge, ANEST IWATA SLP-07EED air compressor and a CKD RP1000-8-07 precision regulator. This setup is identical to the one used in [15], [16] and [18]. Aside from measurements within the normal operating range, additional measurements for 0 and 0.5 MPa are conducted to determine the stiffness beyond the fully extended state.

D. Parametrization

The actuator geometry is described using the design parameters shown in Fig. 1. To achieve a maximum power density the unit's width w and the vertical distances between the McKibben

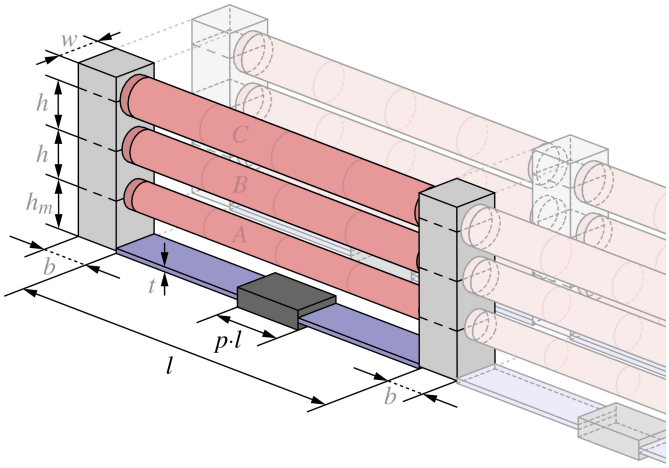

Fig. 1. Parametrized actuator unit geometry. McKibben muscles are shown in red, their tip portions in dark red, the flexure strip in blue, the rigid brackets in light gray and the reinforced section in dark gray. Characters in black depict optimization parameters, in gray manually set parameters and in red the McKibben muscle indices. Serial and parallel units are indicated as half-transparent geometries.

muscles h are set equal to the inflated diameter of the McKibben muscles of 5 mm. To maintain a total height below 20 mm the number of McKibben muscles is limited to three and the height of the first McKibben muscle above the flexure h_m is set to 5 mm. With regards to manufacturing the bracket length b is also chosen to be 5 mm. The flexure thickness t is varied between 0.1 and 0.9 mm. The flexure length l, its reinforced portion p and the initial contraction ratios ε_{init} for each McKibben muscle are the optimization variables constituting the parameter vector.

$$\mathbf{x} = [l,\ p,\ \varepsilon_{init_A},\ \varepsilon_{init_B},\ \varepsilon_{init_C}] \tag{1}$$

The contraction ratio ε is defined as the relative shortening in respect to the uninflated and unstressed state.

$$\varepsilon = 1 - \frac{\l}{\l_0} \tag{2}$$

where $\l$ is the current length of the McKibben muscle and $\l_0$ its length at rest. In case of ε_{init} the length $\l$ equals the flexure length ($\l_{init} = l$) and $\l_0$ is the uninflated length at rest, before assembly. ε_{init} is limited to 0.1806, the maximum contraction ratio $\varepsilon_{\max}$ at 0.5 MPa, to avoid that the fully contracted length at 0.5 MPa exceeds the flexure length.

E. McKibben Muscle Model

McKibben muscles can be regarded as active nonlinear springs, where the stiffness can be controlled by the applied pressure P [32]. However, since in this study we are only concerned with the isobaric behavior at two distinct pressure states, the minimum and maximum operating pressures 0 and 0.5 MPa, respectively, we model the McKibben muscles as passive elements.

Their stiffness behavior is separated into three regions: a region of approximately linear stiffness in the operating range $0 \leq \varepsilon \leq \varepsilon_{\max}$, a region of rapid nonlinear stiffness increase for $\varepsilon < 0$ and a region of rapid nonlinear stiffness decrease for $\varepsilon > \varepsilon_{\max}$. Accordingly, the measurement data between $\varepsilon = 0$ and 0 N tensile force ($\varepsilon = \varepsilon_{\max}$) are fitted using a first order polynomial. The data for $\varepsilon < 0$ are fitted using a third order polynomial.

$$F = \begin{cases} k_{l1}\varepsilon + C, & \text{if } \ \varepsilon \geq 0 \\ k_{nl3}\varepsilon^3 + k_{nl2}\varepsilon^2 + k_{nl3}\varepsilon + C, & \text{if } \ \varepsilon < 0 \end{cases} \tag{3}$$

where F is the tension force exerted by the McKibben muscle, k are the elongation stiffness coefficients and C is a constant depicting the tension force at $\varepsilon = 0$. To obtain a continuous function the constant C is equal for both cases. The rapid stiffness decrease for $\varepsilon > \varepsilon_{\max}$ is achieved by assigning a low bending stiffness to the McKibben muscle elements which leads them to immediately buckle under compressive loads.

When McKibben muscles contract their diameter expands. However, at the tips where the McKibben muscles connect to the brackets the diameter is fixed to its initial value. This results in a region where the diameter transitions from the initial value to the contraction dependent value of the uniformly cylindrical portion. Due to this geometry constraint the deformations at the non-cylindrical tips are restricted which leads to a loss of contraction capability with respect to a purely cylindrical McKibben muscle [32]. This loss can be expressed as a reduction of the McKibben muscle length $\l$ which amounts to twice the difference between the initial radius r_0 and the radius of the cylindrical portion r [33].

$$\l' = \l - 2(r - r_0) \tag{4}$$

where $\l'$ is the corrected length.

F. Simulation

A single actuator unit of the mechanism shown in Fig. 1 is modeled in the flexible multibody dynamics software package SPACAR [34] using finite two-node beam elements, which include geometric nonlinearities and flexibility formulated in discrete deformation modes. The flexure strip is modeled as a chain of flexible beam elements with rectangular cross-section. The brackets and the reinforced section are modeled as rigid beams. When $p \leq 0.01$, the reinforced section is omitted. The McKibben muscles are implemented as chains of beam elements with circular cross-section, which feature the stiffness properties described in subsection II-E. Furthermore, their lengths are corrected using the minimum and maximum radii 1.5 and 2.5 mm, respectively, which yields a tip length of 1 mm reducing the initial McKibben muscle lengths $\l_{init}$ by an absolute value of 2 mm. The McKibben muscle elements are inserted into the model at their corrected minimum contracted length for the given pressure. This is done to achieve zero tension force at that length ($\varepsilon = \varepsilon_{\max}$) as well as buckling for smaller lengths ($\varepsilon > \varepsilon_{\max}$). The inactive tip portions are appended to each side of the McKibben muscles. These feature the same bending stiffness as the active portion but have an infinite elongation stiffness.

With this model kinetostatic simulations are performed to determine the significant characteristics of a specific actuator design. This is done in a two-step procedure, depicted in Fig. 2. First, the McKibben muscles are pre-loaded using rigid beam elements that extend from one end of the contracted McKibben muscles to the bracket. The rigid elements shorten to zero length applying tension to the McKibben muscles. This is equivalent to pressurizing the McKibben muscles, given they were directly connected to the brackets.

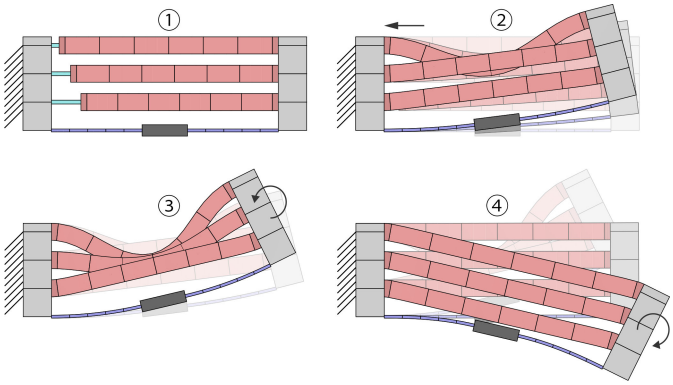

Fig. 2. Two-step simulation procedure. The top two sub-figures show the pre-loading of the McKibben muscles from state 1 to state 2 by shortening the pre-loading beam elements, depicted in teal. The bottom two sub-figures show the primary load case, where the rotation φ is applied to the right bracket - first in positive direction (state 3) and consecutively in negative direction (state 4). Beam element borders are indicated by solid black lines. The remaining color coding is identical to Fig. 1.

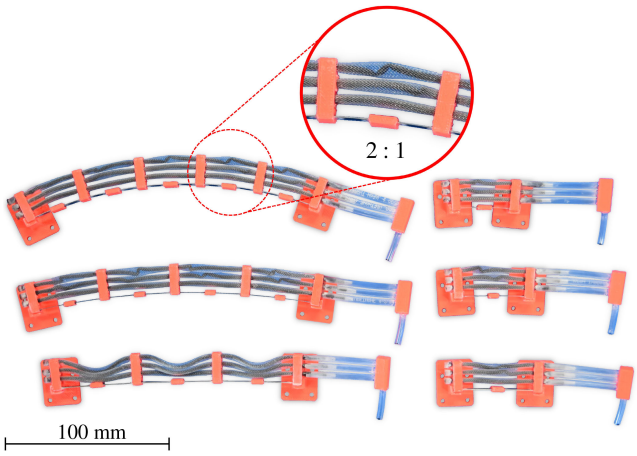

Fig. 3. Test specimens. Multi-unit specimens are shown to the left and the respective single-unit specimens to the right. Flexure thicknesses from top to bottom: $t = 0.3$, 0.4 and 0.5 mm.

This pre-loaded state marks the initial step of the primary load case in which the left bracket of the actuator unit is fixed while the right bracket is rotated by an angle φ which is first applied in positive and consecutively in negative direction. The amount of rotation, i.e., the range of φ is set using the flexure length l and the desired minimum bending radius $\rho^* = 80$ mm, applying an additional 50 % margin.

$$\varphi \quad \in \quad [-1.5\ {}^{l}/_{\rho^*} \ \ldots \ 1.5\ {}^{l}/_{\rho^*}] \text{ rad} \tag{5}$$

G. Optimization

Using the computational model which is described in the previous subsection II-F the mechanism is optimized to maximize the moment M at the position $\varphi = 0$ rad which, given the intended actuator placement, corresponds to an arm elevation angle of 90 deg. Thus, the objective is

$$\boldsymbol{\delta} = M^{-1}_{(\varphi=0)} \tag{6}$$

In order to meet the requirements set in subsection II-A and to obtain a feasible design, penalties $\mathbf{p}$ are multiplied with a penalty coefficient $k_p = 10^5$ and added to the objective. The first penalty applies in case the bending radius ρ does not reach the desired value ρ^* before one of the McKibben muscles is fully extended. The bending radius is determined by fitting a circle tangentially to the centers of the brackets.

$$\mathbf{p_1} = \begin{cases} 0, & \text{if} \quad \rho - \rho^* \leq 0 \\ \rho - \rho^*, & \text{if} \quad \rho - \rho^* > 0 \end{cases} \tag{7}$$

$$\rho = \left(\frac{l}{\varphi_{(\varepsilon=\varepsilon_{\max})}} + ({}^{b}/_{2})^2 \right)^{1/2} \tag{8}$$

The second penalty applies in case the von Mises stress in the flexure exceeds a limit value $\sigma_{\max}$. The von Mises stress is determined for each load step where $0 \leq \varepsilon \leq \varepsilon_{\max}$.

$$\mathbf{p_2} = \begin{cases} 0, & \text{if} \quad \sigma_{mises} - \sigma_{\max} \leq 0 \\ \sigma_{mises} - \sigma_{\max}, & \text{if} \quad \sigma_{mises} - \sigma_{\max} > 0 \end{cases} \tag{9}$$

$$\sigma_{\max} = {}^{\sigma_t}/_{FOS} \tag{10}$$

where σ_t is the tensile strength of the flexure material and $FOS = 1.2$ is applied as a factor of safety.

The cost function for the minimization problem thus becomes

$$f(\mathbf{x}) = \boldsymbol{\delta} + k_p(\mathbf{p_1} + \mathbf{p_2}) \tag{11}$$

According to this cost function ideal parameter sets $\mathbf{x}^*$ are determined using the Genetic Algorithm function *ga()* from the MATLAB Global Optimization Toolbox.

H. Specimens

To validate the simulation and optimization results, physical specimens based on the optimized results for the flexure thicknesses 0.3, 0.4 and 0.5 mm are manufactured and tested. The used materials are described in subsection II-C. Each specimen consists of one flexure, three McKibben muscles and seven individual parts which are produced in ABS via fused deposition modeling on a Zortrax M200 and M300. All parts are joined together using Loctite 401 instant adhesive. Two ABS parts are glued to the flexure which form a brace that contains the stiffeners as well as frames for each bracket. The McKibben muscles are sealed off to one side and routed through and fixed to a chain of $5 \times 5 \times 5$ mm brackets with 3 mm through-holes. For each McKibben muscle the space between the brackets is set according to their computed length at rest l_0. Correct spacing between parts is achieved by thin struts that are removed after assembly. At the open end of the McKibben muscles 50 mm long pieces of polyurethane tube are attached as pressure inlets. The individual tubes lead to an ABS manifold part where they are merged into a single tube which connects to the pressure supply. Subsequently, the brackets are placed inside and glued to the bracket frames. In doing so the correct amount of pre-contraction is applied to each McKibben muscle. At both terminal points of the actuator interface parts are attached, which are used to mount the actuator to the test setup using M3 bolts.

For each flexure thickness one actuator consisting of a single unit and one consisting of multiple units is produced. The number of units is determined such that the actuator can attain a total deflection of at least ± 90 deg. All six tested physical specimens are shown in Fig. 3.

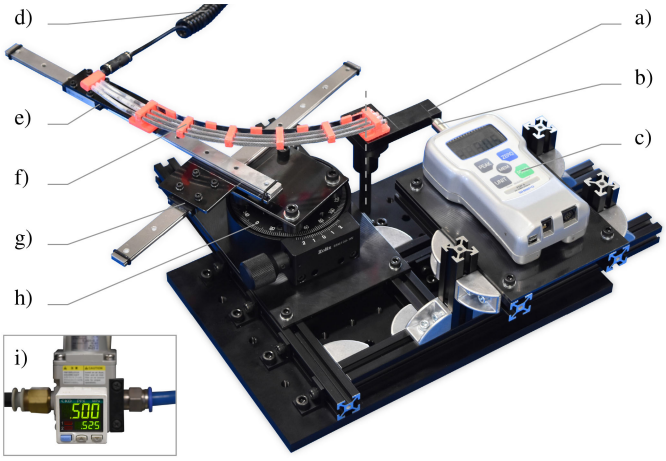

Fig. 4. Experimental setup to measure the pressure and angle dependent moments. (a) lever (rotary axis indicated by dashed line), (b) conical tip, (c) force gauge, (d) coiled tube (pressure supply), (e) linear guide 1, (f) specimen, (g) linear guide 2, (h) manual rotary stage, (i) regulator.

I. Test Setup

To test the angle dependent moment characteristic of each actuator a dedicated test setup, shown in Fig. 4, is built which emulates the load conditions set in the simulation. The test specimen is fixed on one end to a linear guide, connected to a second linear guide which is oriented perpendicular to the first and in turn is connected to a Zolix Instruments RSM100-1 W manual rotary stage. This arrangement enables the application of precise rotations without imposing translational constraints within the plane. Therefore, only a moment is transmitted and measured. The other end is fixed to a lever made from 10 mm thick steel plate which rests on a flange that connects to a shaft via two ball bearings. The rotation of the lever is unilaterally blocked by a Nidec-Shimpo FGP-5 digital force gauge which connects to the lever via a cone shaped tip which is placed at a distance of 50 mm from the rotation axis. In this way, the moments exerted by the actuator onto the lever can be accurately measured. All elements of the test setup connect to each other via 3 mm thick steel mounting plates, 20×20 mm aluminum extrusions and a 10 mm thick aluminum optical plate which forms the base of the setup. Pressure to the McKibben muscles is supplied through a coiled tube which is suspended from the ceiling to minimize external moments and forces exerted onto the test setup. The pressure is supplied by a ANEST IWATA SLP-07EED air compressor and controlled using a CKD RP1000-8-07 precision regulator.

J. Experiment

Using this test setup all six test specimens are characterized under quasistatic conditions at inlet pressures of 0 and 0.5 MPa. The specimens are fixed to the setup at a zero deflection angle and the inlet pressure is set to the specified value using the regulator. The angle is manually adjusted in intervals of 2 and 5 deg for the single-unit and the multi-unit specimens, respectively, and the force is read from the force gauge display. First, the angle is adjusted from its initial position at the zero angle to the minimum negative angle, then to the maximum positive angle, and back to the zero angle. These minimum and maximum angles are either the values of maximum von Mises stress as determined in simulation for the specific specimen or are dictated by the test setup which is limited to a range of -35 to 100 deg, before its components collide. The procedure is repeated five times for each specimen and the data of the five measurements are averaged to obtain the characteristic angle to moment behavior of the respective actuator.

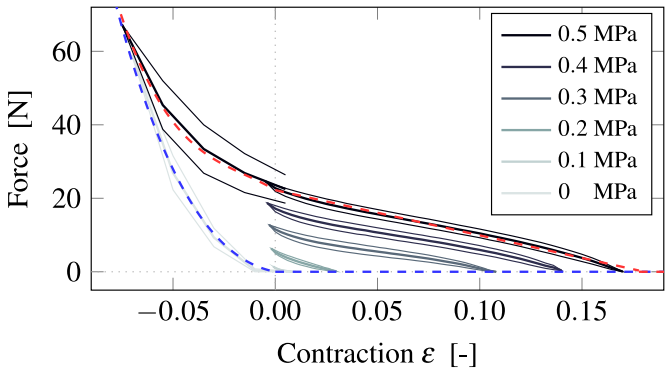

Fig. 5. Isobaric McKibben muscle stiffness. The thin solid lines represent the mean of five consecutive measurements (counter-clockwise direction), the thick solid lines their average, i.e., the center of the hysteresis field. The blue and the red dashed lines show the fitted stiffness models for 0 and 0.5 MPa, respectively, which are used in the simulations.

TABLE I
McKibben Muscle Stiffness Model

P MPa	k_{l1} N/ε	k_{nl3} N/ε³	k_{nl2} N/ε²	k_{nl1} N/ε	C N
0.5	-123.03	-127033	-5669.1	-337.5	22.219
0	0	-57212	6090.7	-110.71	0

TABLE II
Optimized Parameters

t mm	l m	p -	ε_{init_A} -	ε_{init_B} -	ε_{init_C} -	$M_{(\varphi=0)}$ Nm
0.9	0.0132	0.0008	0.1576	0.1653	0.1796	0.0344
0.8	0.0319	0.0535	0.0578	0.1106	0.1596	0.1999
0.7*	0.0451	0.0557	0.0471	0.1008	0.1489	0.2380
0.6*	0.0495	0.0202	0.0408	0.094	0.1421	0.2630
0.5*	0.0453	0.1566	0.0489	0.0994	0.1467	0.2431
0.4	0.0389	0.1569	0.0472	0.1014	0.1498	0.2347
0.3	0.0311	0.2699	0.0547	0.1074	0.155	0.2100
0.2	0.025	0.7064	0.0625	0.1149	0.1645	0.1826
0.1	0.0183	0.8103	0.0721	0.1203	0.1711	0.1540

*McKibben muscle intersecting flexure in simulation.

III. Results

The stiffness of the McKibben muscle, measured according to subsection II-C, as well as the modeled stiffness are shown in Fig. 5. The parameters of the stiffness model fitted according to subsection II-E are presented in Table I.

The optimized parameters and moments at $\varphi = 0$ rad for the individual actuator configurations are given in Table II. Several trends can be observed. With increasing flexure thickness t, the moment $M_{(\varphi=0)}$ and the length l increase. Conversely, with the exception of $t = 0.5$ and 0.4 mm which have similar values, the relative size of the stiffener section p decreases and the values

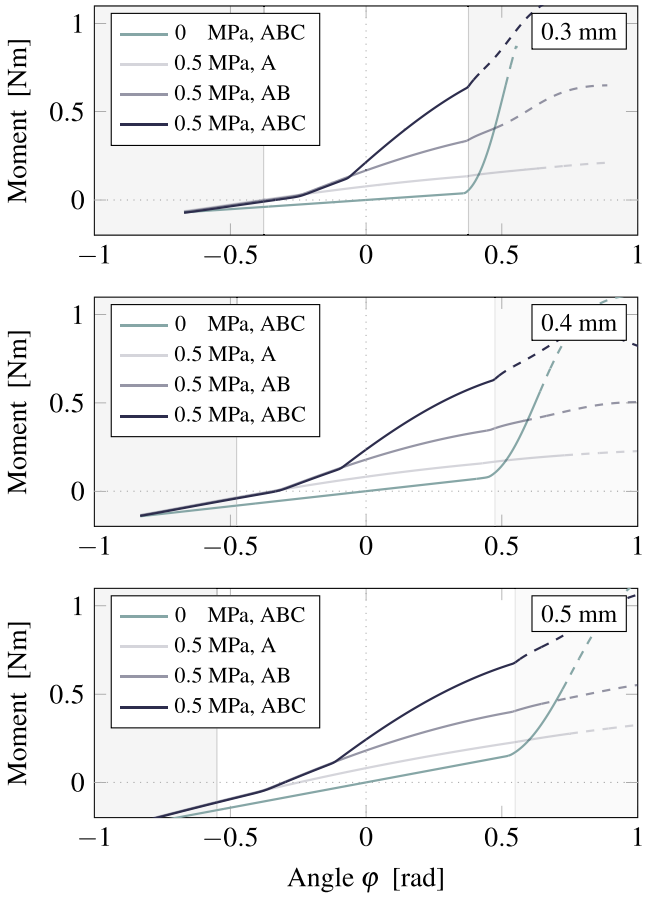

Fig. 6. Simulated moment response curves. From top to bottom: $t = 0.3$, 0.4 and 0.5 mm. The solid lines transition into dashed lines at the point where the maximum von Mises stress is exceeded. The normal operating range, i.e., the range in which the absolute bending radius $|\rho|$ is ≥ 80 mm, is highlighted by a white background while the shaded areas indicate the regions outside of this range. The thin dotted lines indicate $\varphi = 0$ and $M = 0$, respectively. From this figure it can be seen that the McKibben muscles start contributing to the overall stiffness at different angles, beginning with muscle A and ending with muscle C, shortly before $\varphi = 0$. The stiffness added by each consecutive McKibben muscle increases with respect to the prior ones. Beyond the upper end of the operating range a rapid increase in stiffness can be observed for the ABC curves, while the AB curves exhibit only a slight and the A curves no increase, which points to McKibben muscle C being the main cause.

of ε_{init} also decrease. However, all these trends are broken and mostly reversed at $t \geq 0.7$ mm.

The simulated angle dependent moment curves of the optimized designs for $t = 0.3$, 0.4 and 0.5 mm are shown in Fig. 6. To illustrate the contribution of each McKibben muscle to the total moment of the actuator, the figure also shows simulation data for the cases when either only McKibben muscle A, or the combination of McKibben muscles A and B are used in the computational model. To further exemplify this Fig. 7 shows the angle dependent tension force of each McKibben muscle for all three flexure thicknesses.

The experimental results for the specimens with $t = 0.3$, 0.4 and 0.5 mm thickness are shown in Fig. 8. The respective measured moments at the straight position ($\varphi = 0$) are 0.246, 0.256 and 0.312 Nm for the single-units and 0.220, 0.274 and 0.270 Nm for the multi-units. The physical geometries have been measured, revealing that the value of h_m in all test specimens is significantly larger by 0.71, 0.76 and 0.85 mm (14.2 %, 15.1 % and 17.1 %), respectively. Therefore, simulations with adjusted h_m are conducted and presented as well in Fig. 8. The root-mean-square errors (RMSE) between the measurements and the corrected simulation data are presented in Fig. 8 and are in the range between 0.013 and 0.049 Nm.

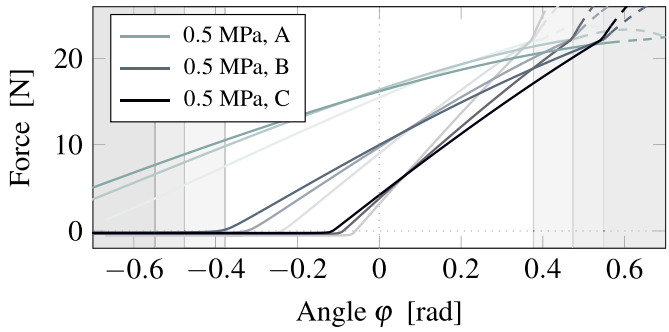

Fig. 7. Simulated force response curves. From light to dark: $t = 0.3$, 0.4 and 0.5 mm. The solid lines transition into dashed lines at the point where the maximum von Mises stress is exceeded. The shaded areas adhere to the same color grading and indicate the respective regions outside of the normal operating range. The thin dotted lines indicate $\varphi = 0$ and $F = 0$, respectively. This figure shows that optimized designs are characterized by the force curves of all McKibben muscles intersecting at a point close to the end of their respective operating range, after which the stiffness of muscles A and B increases. The force exerted at these intersection points is similar across all McKibben muscles and optimized designs, yet occurring at different angles.

To illustrate of a potential application of the actuator, a wearable proof-of-concept prototype based on the optimized design for $t = 0.4$ mm was built and is shown in Fig. 9. Its unilateral actuator is 80 mm wide, giving it a theoretical moment output of 3.76 Nm at 90 deg arm elevation which is 41 % of the required moment to lift a fully extended arm.

IV. Discussion

The results support that the presented synthesis method is suitable to obtain bending actuators with maximized moment outputs for a given set of components. Generally, it can be stated that a larger flexure thickness increases the buckling resistance and bending stiffness, but also the bending stress at a given bending radius. Due to the increase in buckling resistance, the flexure itself can withstand higher compressive forces exerted by the McKibben muscles. Furthermore, the McKibben muscles together with the flexure can become longer and the reinforced section shorter. This allows for a larger moment at $\varphi = 0$ rad, while maintaining the necessary ROM. Adversely affecting this, however, is the bending stress which for flexure thicknesses $t \geq 0.7$ mm and the required minimum bending radius of $\rho^* \leq 80$ mm apparently becomes the limiting factor to the acquirable moment at $\varphi = 0$ rad. The effect of increasing bending stiffness is ambivalent. While it passively provides a moment that counteracts gravity, and thereby relieving the McKibben muscles and lowering the energy requirement, it could become disadvantageous in an assistive device, if considerable force is required by the user to reach the full natural ROM. The flexure thicknesses $t = 0.3$, 0.4 and 0.5 mm were chosen for evaluation, as their stiffnesses appeared to lie within a favorable range.

For longer flexure lengths the simulation showed intersection of the flexure and McKibben muscle A. To avoid this an intersection penalty could be added, contact modeled and h_m adjusted or used as a design variable. However, for the specimens with

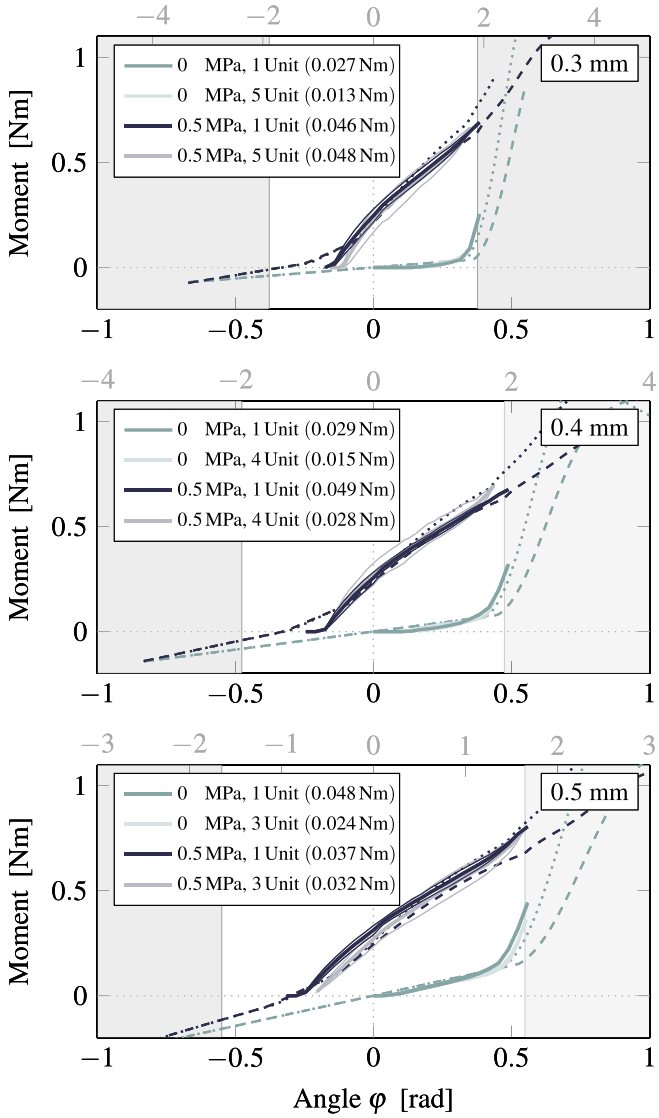

Fig. 8. Experimental results. From top to bottom $t = 0.3$, 0.4 and 0.5 mm. The thin solid lines represent the mean of five consecutive measurements (clockwise direction), the thick solid lines their average, i.e., the center of the hysteresis field. The dashed lines show the simulated moment curves using the optimized parameters. The dotted lines show the simulated moment curves using the measured values for the parameter h_m. The normal operating range is highlighted by a white background while the shaded areas indicate the regions outside of this range. The thin dotted lines indicate $\varphi = 0$ and $M = 0$, respectively. The multi-unit result angles are divided by the number of units. Their actual angles are indicated in gray on the top. The root-mean-square error (RMSE) for each measurement with respect to the corrected simulation data (dotted line) is shown in brackets. These results show that the experimental results for both single units and multiple units generally show good agreement with the simulated results, if the measured geometric dimensions of the physical specimens are used in the computational model.

flexure thickness $t = 0.5$ mm no negative effect of this could be observed during experiments.

With respect to the experimental validation some uncertainties remain. In the tension tests it was difficult to determine the exact absolute position that corresponds to a zero contraction ratio. Consequently, the measured stiffness curves, shown in Fig. 5, may be slightly shifted along the x-axis with respect to reality. This, along with the manufacturing inaccuracies are probably the main reasons for the discrepancies between the simulated

Fig. 9. Wearable proof-of-concept prototype worn by a healthy subject. This figure illustrates the actuator's potential to achieve close alignment to the body and an overall small size of the resulting assistive device.

and the measured behavior of the actuators. In comparison to the initial predictions the moments at $\varphi = 0$ rad are 5 to 28 % higher and the onsets of the rapidly increasing stiffness occur up to 7 and 21 deg earlier for the single-unit and multi-unit specimens, respectively. Adjusting the parameter h_m according to the measured geometry improved the match to a maximum deviation of 4 and 11 deg, respectively.

The wearable prototype illustrates the potential of this actuator design regarding its size and close-to-body alignment. However, using our currently available components it is likely too weak for practical purposes. By using the design for $t = 0.6$ mm its theoretical moment output could be raised to 4.21 Nm, i.e., 46 % of the required moment.

Considering the values of ε_{init_C} which all approach the limit $\varepsilon_{\max} = 0.1806$, adding a fourth McKibben muscle of the same type does not seem a feasible option to further increase the moment at $\varphi = 0$ rad. Therefore, to improve the performance the active components need to be revised. To this end, the maximum contraction ratios of the McKibben muscles could be customized according to their height above the flexure, e.g. by adjusting the braid angles. This would potentially also enable the use of additional McKibben muscles along the height. Alternatively, the pneumatic McKibben muscles may be replaced by more powerful alternatives, such as hydraulic artificial muscles and cable-based actuation systems.

The actuator concept can potentially be applied to other joints of the human body. This, however, will in most cases require the actuator to be optimized for different bending angles and bending radii. If two-way actuation is required, McKibben muscles could be placed to either side of the actuator, or an antagonistic pair of unilaterally acting actuators could be used.

V. Conclusion

The pneumatic bending actuator proposed in this letter is the first to combine McKibben muscles with flexures, resulting in a leveraged large rotational range of motion and reduced localized forces at the attachments. A method is presented to optimize the actuator design towards a maximum output moment, given a set of basic components and initial design specifications. The computational results are verified by experiments, displaying the ability of this actuator to provide assistance while allowing for a natural range of motion in the actuated degree of freedom. Its close-to-body alignment and potential for building small size upper-limb assistive wearable robots is illustrated by means of a proof-of-concept prototype. When employed on an upper-limb wearable robot and given a width of 80 mm, the optimized

designs can theoretically produce a moment of up to 4.21 Nm at 90 deg arm elevation.

ACKNOWLEDGMENT

The content of this publication is the sole responsibility of the authors. Neither the Japan Society for the Promotion of Science, nor the European Commission or its services can be held responsible for any use that may be made of the information it contains.

REFERENCES

[1] R. J. Varghese, D. Freer, F. Deligianni, J. Liu, and G.-Z. Yang, "Chapter 3 - Wearable robotics for upper-limb rehabilitation and assistance: A review of the state-of-the-art, challenges, and future research," in *Wearable Technology in Medicine and Health Care*, R. K.-Y. Tong, Ed., New York, NY, USA: Academic, 2018, pp. 23–69.

[2] A. J. Veale and S. Q. Xie, "Towards compliant and wearable robotic orthoses: A review of current and emerging actuator technologies," *Med. Eng. Phys.*, vol. 38, no. 4, pp. 317–325, 2016.

[3] S. K. Manna and V. N. Dubey, "Comparative study of actuation systems for portable upper limb exoskeletons," *Med. Eng. Phys.*, vol. 60, pp. 1–13, 2018.

[4] P. Maciejasz, J. Eschweiler, K. Gerlach-Hahn, A. Jansen-Troy, and S. Leonhardt, "A survey on robotic devices for upper limb rehabilitation," *J. NeuroEng. Rehabil.*, vol. 11, no. 1, Jan. 2014, Art. no. 3.

[5] L. A. van der Heide, B. van Ninhuijs, A. Bergsma, G. J. Gelderblom, D. J. van der Pijl, and L. P. de Witte, "An overview and categorization of dynamic arm supports for people with decreased arm function," *Prosthetics Orthotics Int.*, vol. 38, no. 4, pp. 287–302, 2014, pMID: 23950551.

[6] R. Gopura, D. Bandara, K. Kiguchi, and G. K. I. Mann, "Developments in hardware systems of active upper-limb exoskeleton robots: A review," *Robot. Auton. Syst.*, vol. 75, pp. 203–220, 2016.

[7] O. Plos, S. Buisine, A. Aoussat, F. Mantelet, and C. Dumas, "A universalist strategy for the design of assistive technology," *Int. J. Ind. Ergonom.*, vol. 42, no. 6, pp. 533–541, 2012.

[8] C.-Y. Chu and R. M. Patterson, "Soft robotic devices for hand rehabilitation and assistance: A narrative review," *J. NeuroEng. Rehabil.*, vol. 15, no. 1, 2018, Art. no. 9.

[9] F. Daerden and D. Lefeber, "Pneumatic artificial muscles: Actuators for robotics and automation," *Eur. J. Mech. Environ. Eng.*, vol. 47, Mar. 2002.

[10] Ching-Ping Chou and B. Hannaford, "Measurement and modeling of McKibben pneumatic artificial muscles," *IEEE Trans. Robot. Autom.*, vol. 12, no. 1, pp. 90–102, Feb. 1996.

[11] M. D. Volder, A. Moers, and D. Reynaerts, "Fabrication and control of miniature McKibben actuators," *Sensors Actuators A: Phys.*, vol. 166, no. 1, pp. 111–116, 2011.

[12] M. Takaoka, K. Suzumori, S. Wakimoto, K. Iijima, and T. Tokumiya, "Fabrication of thin McKibben artificial muscles with various design parameters and their experimental evaluations," in *Proc. 5th Int. Conf. Manuf. Mach. Des. Tribology*, 2013, p. 82.

[13] K. P. Ashwin and A. Ghosal, "A survey on static modeling of miniaturized pneumatic artificial muscles with new model and experimental results," *Appl. Mech. Rev.*, vol. 70, no. 4, pp. 040 802–040 802–20, Oct. 2018.

[14] S. Kurumaya, H. Nabae, G. Endo, and K. Suzumori, "Design of thin McKibben muscle and multifilament structure," *Sensors Actuators A: Phys.*, vol. 261, pp. 66–74, 2017.

[15] S. Koizumi, S. Kurumaya, H. Nabae, G. Endo, and K. Suzumori, "Braiding thin McKibben muscles to enhance their contracting abilities," *IEEE Robot. Autom. Lett.*, vol. 3, no. 4, pp. 3240–3246, Oct. 2018.

[16] T. Abe *et al.*, "Fabrication of 18 weave muscles and their application to soft power support suit for upper limbs using thin McKibben muscle," *IEEE Robot. Autom. Lett.*, vol. 4, no. 3, pp. 2532–2538, Jul. 2019.

[17] Y. Funabora, "Flexible fabric actuator realizing 3D movements like human body surface for wearable devices," in *Proc. IEEE/RSJ Int. Conf. Intell. Robots Syst.*, Oct. 2018, pp. 6992–6997.

[18] T. Hiramitsu, K. Suzumori, H. Nabae, and G. Endo, "Experimental evaluation of textile mechanisms made of artificial muscles," in *Proc. 2nd IEEE Int. Conf. Soft Robot.*, Apr. 2019, pp. 1–6.

[19] T. Abe, S. Koizumi, H. Nabae, G. Endo, and K. Suzumori, "Muscle textile to implement soft suit to shift balancing posture of the body," in *Proc. IEEE Int. Conf. Soft Robot.*, Apr. 2018, pp. 572–578.

[20] H. Kobayashi, Y. Ishida, and H. Suzuki, "Realization of all motion for the upper limb by a muscle suit," in *Proc. RO-MAN 13th IEEE Int. Workshop Robot Human Interactive Commun.*, 2004, pp. 631–636.

[21] A. Ohno, H. Nabae, and K. Suzumori, "Static analysis of powered low-back orthosis driven by thin pneumatic artificial muscles considering body surface deformation," in *Porc. IEEE/SICE Int. Symp. Syst. Integration*, Dec. 2015, pp. 39–44.

[22] T. Noritsugu, "Pneumatic soft actuator for human assist technology," in *Proc. 6th JFPS Int. Symp. Fluid Power*, Nov. 2005, pp. 11–20.

[23] B. Wang, K. C. Aw, M. Biglari-Abhari, and A. McDaid, "Design and fabrication of a fiber-reinforced pneumatic bending actuator," in *Proc. IEEE Int. Conf. Adv. Intell. Mechatronics*, Jul. 2016, pp. 83–88.

[24] A. Oosterwijk, M. Nieuwenhuis, C. van der Schans, and L. Mouton, "Shoulder and elbow range of motion for the performance of activities of daily living: A systematic review," *Physiotherapy Theory Practice*, vol. 34, no. 7, pp. 505–528, 2018, pMID: 29377745.

[25] P. de Leva, "Adjustments to Zatsiorsky-Seluyanov's segment inertia parameters," *J. Biomech.*, vol. 29, no. 9, pp. 1223–1230, 1996.

[26] I. A. Murray and G. R. Johnson, "A study of the external forces and moments at the shoulder and elbow while performing every day tasks," *Clin. Biomech.*, vol. 19, no. 6, pp. 586–594, Jul. 2004.

[27] A. G. Dunning and J. L. Herder, "A review of assistive devices for arm balancing," in *Proc. IEEE 13th Int. Conf. Rehabil. Robot.*, Jun. 2013, pp. 1–6.

[28] C. Zeagler, M. Gandy, and P. M. Baker, "The assistive wearable: Inclusive by design," *Assistive Technol. Outcomes Benefits*, vol. 12, pp. 11–36, 2018.

[29] A. R. Tilley and Henry Dreyfuss Associates, *The Measure of Man and Woman: Human Factors in Design, Revised Edition*. Whitney Library of Design, Dec. 2001.

[30] *Hardness Tests and Hardness Number Conversions*, SAE International, Standard, Jan. 2018.

[31] *Z-ULTRAT Technical Data Sheet*, Zortrax S.A., Jan. 2018. [Online]. Available: https://cf.zortrax.com/wp-content/uploads/2018/06/Z-ULTRAT_Technical_Data_Sheet_eng.pdf

[32] B. Tondu, "Modelling of the McKibben artificial muscle: A review," *J. Intell. Mater. Syst. Struct.*, vol. 23, no. 3, pp. 225–253, 2012.

[33] C. S. Kothera, M. Jangid, J. Sirohi, and N. M. Wereley, "Experimental characterization and static modeling of McKibben actuators," *J. Mech. Des.*, vol. 131, no. 9, pp. 091 010–091 010–10, Aug. 2009.

[34] J. B. Jonker and J. P. Meijaard, *SPACAR — Computer Program for Dynamic Analysis of Flexible Spatial Mechanisms and Manipulators*. Berlin, Germany: Springer, 1990, pp. 123–143.